JOURNAL OF GEOPHYSICAL RESEARCH, VOL. 115, D11204, doi:10.1029/2009JD012635, 2010

Morphological characterization of soot aerosol particles during LACIS Experiment in November (LExNo)

A. Kiselev,[1] C. Wennrich,[1] F. Stratmann,[1] H. Wex,[1] S. Henning,[1] T. F. Mentel,[2] A. Kiendler-Scharr,[2] J. Schneider,[3] S. Walter,[3] and I. Lieberwirth[4]

Received 12 June 2009; revised 11 January 2010; accepted 21 January 2010; published 4 June 2010.

[1] Combined mobility and aerodynamic measurements were used to characterize the morphology of soot particles in an experimental campaign on the hygroscopic growth and activation of an artificial biomass burning aerosol. A custom-made, single-stage low-pressure impactor and two aerosol mass spectrometers (AMS) operating in the free molecular regime were used to measure the vacuum aerodynamic diameter of mobility-selected artificial soot particles that were produced in a spark discharge generator and then modified by condensation of ammonium hydrogen sulfate or levoglucosan as a coating to change their hydroscopic activity. Transmission electron microscope images revealed a relationship between the electrical mobility diameter and the diameter of the enveloping sphere, thus enabling evaluation of the effective density of soot agglomerates. A fractal description of the morphology of the soot aggregates allowed for evaluation of the average mass of the hygroscopic material per particle. The average mass of the hygroscopic material per particle was also measured directly with the two AMS instruments, and the agreement between the two methods was found satisfactory. This tandem approach allows detection of small changes in the particle effective density and morphology caused by condensation of organic material.

Citation: Kiselev, A., C. Wennrich, F. Stratmann, H. Wex, S. Henning, T. F. Mentel, A. Kiendler-Scharr, J. Schneider, S. Walter, and I. Lieberwirth (2010), Morphological characterization of soot aerosol particles during LACIS Experiment in November (LExNo), *J. Geophys. Res.*, *115*, D11204, doi:10.1029/2009JD012635.

1. Introduction

[2] Current development of experimental aerosol science tends toward simultaneous characterization of aerosol systems with respect to their morphology, chemical composition, optical properties and interaction with its atmospheric environment. Recent advances in measurement techniques enable quantification of relationships among size, shape, composition, density, hygroscopicity and cloud condensation nuclei (CCN) activity of an aerosol.

[3] Such a comprehensive approach is governed by the need to clarify the relationships among chemical composition, microphysical properties, and hygroscopic properties of particles. Such relationships can be particularly complicated in the case of a biomass burning aerosol, in which properties and composition can vary widely according to the type of biomass, local atmospheric conditions and subsequent ageing processes.

[4] In 2005 the LACIS Experiment in November (LExNo) took place at the Leipzig Aerosol and Cloud Interaction Simulator (LACIS), an experimental facility built to study the hygroscopic properties and CCN activity of aerosol particles of different nature [*Stratmann et al.*, 2004]. A thorough description of the LExNo experiment is given in the companion overview paper of *Stratmann et al.* [2010]. The main goal of LExNo was to clarify the processes that govern the activation and hygroscopic growth of a combustion aerosol. Real biomass burning particles show wide variability in their morphology and chemical composition. To avoid this variability, LExNo involved artificial soot particles that were produced using a PALAS GfG spark discharge generator and then coated by condensation of two different water-soluble substances (ammonium sulfate and levoglucosan) at various quantities and combinations. These coating substances were chosen because they are abundant in atmospheric aerosols and are characteristic of biomass burning aerosols in particular. To study possible effects of the structure of the insoluble core of internally mixed particles on their hygroscopic behavior and activation, the soot particles were compacted prior to coating.

[5] To determine the relationship between the morphology and hygroscopic properties of the soot particles, a comprehensive morphological characterization of the soot particles was required. Numerous publications (e.g., review on the

[1]Institute for Tropospheric Research, Department of Physics, Leipzig, Germany.
[2]ICG-II: Troposphere, Research Centre Juelich, Juelich, Germany.
[3]Particle Chemistry Department, Max Planck Institute for Chemistry, Mainz, Germany.
[4]Max Planck Institute for Polymer Research, Mainz, Germany.

0148-0227/10/2009JD012635

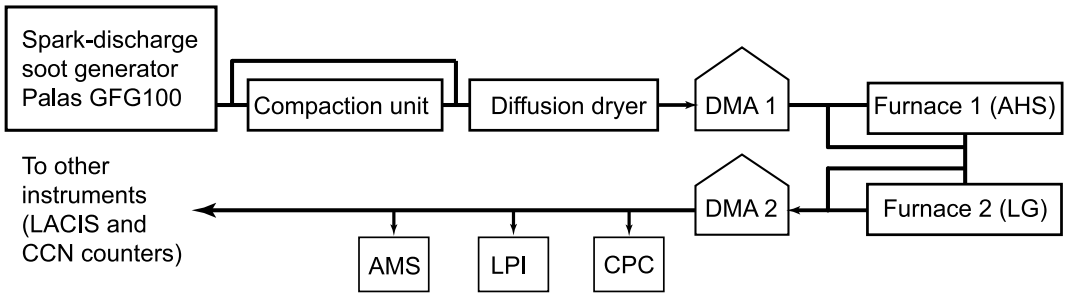

Figure 1. Setup for particle generation and morphology characterization of uncoated and coated artificial soot particles.

tandem measurements by *Park et al.* [2008] and also *DeCarlo et al.* [2004], *Geller et al.* [2006], *McMurry et al.* [2002], *Park et al.* [2003a, 2003b], *Ristimäki et al.* [2002], *Schmidt-Ott* [1988a], *Slowik et al.* [2004], *Van Gulijk et al.* [2004], and *Zelenyuk et al.* [2008a]) show that combined measurements of different size equivalents (e.g., volume, mass, mobility, or projection equivalent size from Transmission Electron Microscope (TEM) image analysis) can be used in estimating the morphology parameters that are not directly measurable (e.g., effective density, fractal dimension, dynamic shape factor). Tandem measurement of particle mobility and aerodynamic equivalent diameters has grown in popularity due to the recent advantages of particle time-of-flight mass spectrometry. An aerosol mass spectrometer (AMS) not only provides chemical characterization of the nonrefractory component of particles, but also determines their aerodynamic diameters. A comprehensive review of the theory behind the tandem method is given by *DeCarlo et al.* [2004] and *Schmid et al.* [2007]. Highly accurate measurements of particle effective density and shape factors by the single-particle mass spectrometer SPLAT were reported recently by *Zelenyuk et al.* [2006] for aggregates of latex microspheres and for nonspherical particles of ammonium sulfate and NaCl. The method of determination of fractal dimension and effective density of combustion-generated soot from the tandem DMA and AMS measurements is described by *Slowik et al.* [2004] and *Schneider et al.* [2006]. In LExNo we also adopted the tandem approach, but used two different instruments to size the particles aerodynamically: an AMS and a custom-made single-stage low-pressure impactor (LPI) [*Kütz and Schmidt-Ott*, 1990]. We also used statistical analysis of TEM images of the soot particles sampled at different stages of the experiment to supply additional morphological information. Our prime objective was to show that the combination of these measurement techniques provides a method sensitive enough to detect changes in the particle morphology that are caused by condensation of water-soluble materials and to evaluate quantitatively the mass of condensed substance per particle. Based on our results, this tandem method revealed an empirical relationship among the mass of coating material, coating conditions, and type of particles being coated, and results from the tandem mobility and aerodynamic measurements are consistent with those obtained from mass spectra measured using AMS instruments.

[6] This paper focuses on morphological characterization of coated soot particles and is part of a series of papers describing the hygroscopic properties and CCN activation of coated soot aerosols [*Stratmann et al.*, 2010; *Henning et al.*, 2010; *Snider et al.*, 2010].

2. Experimental Setup

[7] Detailed description of the LExNo experiment can be found in the overview paper by *Stratmann et al.* [2010]. This section briefly describes the instruments and experimental methods relevant for the characterization of the particle morphology. Figure 1 shows a schematic of the experimental setup for particle generation and morphology characterization.

[8] An artificial soot aerosol was produced by a high-frequency spark discharge generator (GFG 1000, Palas, Germany) with graphite electrodes. The generator was operated with nitrogen as the carrier gas at a flow rate of 5 l/min and at a discharge frequency of 250 Hz. The particles produced under such conditions are loose aggregates consisting of several hundreds of primary particles [*Helsper et al.*, 1993; *Mikhailov et al.*, 2001]. These primary particles are several nanometers in size and consist mostly of amorphous graphite with inclusion of small crystalline packets. A soot aggregate is often characterized by the radius of gyration R_g, which is equal to a mass-weighted root mean square of distances of the primary particles relative to the center of mass of the aggregate. The structure of soot aggregates exhibits fractal-like features and can be statistically described by a power law relationship between the number of primary particles N_{pp} and R_g normalized to the diameter of the primary particle d_{pp} [*Schmidt-Ott*, 1988b; *Wiltzius*, 1987],

$$N_{pp} = k_f \cdot \left(\frac{2 \cdot R_g}{d_{pp}}\right)^{D_f}, \quad (1)$$

where D_f is the average fractal dimension and k_f is the fractal prefactor of the system of agglomerates.

[9] The effect of the soot particle morphology on the activation behavior was studied by changing the packing density of primary particles within an aggregate (compacting) or/and depositing water soluble substances (ammonium sulfate or levoglucosan) on the soot aggregates (coating). Uncompacted soot aggregates (UCS) and soot particles compacted with propanol (PCS) were coated either with ammonium hydrogen sulfate (AHS) or levoglucosan (LG). Thus, a total of four different types of particles were studied: UCS/AHS, USC/LG, PCS/AHS, and PCS/LG. Compaction

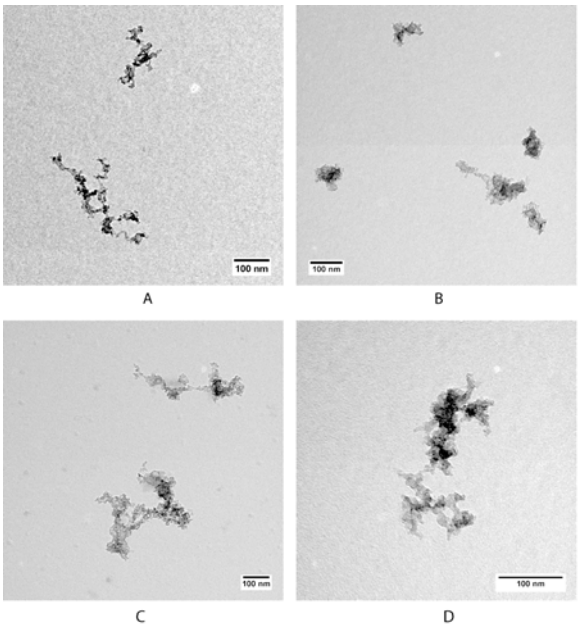

Figure 2. TEM pictures of artificial synthetic soot particles: (a) uncompacted soot particles (UCS), (b) propanol-compacted soot particles (PCS), (c) uncompacted soot coated with ammonium hydrogen sulfate (UCS/AHS), and (d) uncompacted soot coated with levoglucosan (UCS/LG).

of the soot particle was achieved as described by *Kütz and Schmidt-Ott* [1990] and *Schmidt-Ott* [1988a] by condensing propanol vapor on the soot agglomerates with subsequent removal of liquid propanol in an activated charcoal diffusion dryer. Restructuring of the aggregates occurs due to capillary forces acting on branches of the aggregates during the condensation-evaporation cycle [*Mikhailov et al.*, 1999]. Therefore, if no compaction was desired for the aggregates, then the propanol compaction unit was bypassed.

[10] The soot particles from the Palas GfG 1000 generator were selected using a DMA (Differential Mobility Analyzer) according to their electrical mobility. The voltage of the DMA was set to select particles with mobility diameter D_m of 100 nm. The coating was applied to these selected particles by passing the particle containing flow through a heated tubular furnace containing a small amount of coating substance. The ammonium hydrogen sulfate coating was produced by heating ammonium sulfate to between 93°C to 170°C. Analysis of the AMS data revealed a molar ratio of NH_4 to SO_4 of about 1 over the entire temperature range of the furnace. Because the molar ratio for pure ammonium sulfate $(NH4)_2SO_4$ is expected to be equal to 2, this finding suggests that the main coating component was ammonium hydrogen sulfate (NH_4HSO_4). Thermal decomposition of ammonium sulfate is thought to be the reason. (Accordingly, the abbreviation "AHS" is used here to designate the ammonium hydrogen sulfate coating.) The LG coating was applied by heating levoglucosan to between 80°C and 106°C (for details see *Stratmann et al.* [2010]). No thermal decomposition of levoglucosan was observed.

[11] A second DMA after the coating section was used to ensure a constant particle mobility diameter at 84 nm for all the experiments discussed below, unless specified otherwise. Thus, the average coating mass per particle m_{coat} was controlled exclusively by the temperature of the respective coating furnace. The size-selected soot particles were then analyzed using different characterization techniques: (1) amount and chemical composition of the coating was analyzed by using two AMS instruments (Aerodyne Research [*Canagaratna et al.*, 2007]) to measure the mass concentrations of ammonium, sulfate, and total organics; (2) vacuum aerodynamic equivalent diameter D_{vae} of soot aggregates was measured using an a single-stage LPI, custom manufactured at the Institute for Mechanical Engineering, University of Karlsruhe, Germany [*Hering et al.*, 1978, 1979], and also using the two AMS instruments to detect the nonrefractory organic compounds of the soot particles; (3) particle morphology was analyzed using TEM (FEI Tecnai G^2 F20) for soot particles deposited onto carbon-coated copper grids by using a thermophoretic precipitator as described by *Messerer et al.* [2003]; and (4) hygroscopic growth and activation properties of all four aerosol types (UCS/AHS, USC/LG, PCS/AHS, and PCS/LG) were evaluated using LACIS, three CCN counters of different types and a High Humidity Tandem DMA (HHTDMA) system.

[12] The data obtained from the first three analyses are the subject of this paper. The fourth analysis, namely, hygroscopic growth/activation results, are reported in the companion paper by *Henning et al.* [2010].

3. Evaluation of Experimental Data

3.1. Evaluation of TEM Data

[13] TEM samples were collected to examine changes in soot particle morphology due to compaction in the propanol vapor and coatings. Due to the low electron density and relatively high volatility of the coating substances it was not possible to evaluate either the total amount or the spatial distribution of the coating substance inside the aggregates. Therefore the effect of the coating could only be evaluated indirectly by analyzing the rearrangement of the soot aggregate structure after the coating. Figure 2 shows representative images for the four different types of particles (UCS/AHS, USC/LG, PCS/AHS, and PCS/LG.). The coating apparently led to the compaction of the soot agglomerates, similar to the effect of propanol compaction. However, of the visual assessment of the TEM images suggested that the effect was more pronounced in the propanol compaction. The TEM images were mostly obtained at high resolution and therefore not readily suitable for statistically significant estimation of fractal dimension, thus making it impossible to compare the degree of compaction for the different coating materials.

[14] The size distribution of the primary particles d_{pp} (Figure 3a), however, could be measured from the TEM images. The modal value of $d_{pp} = (7.6 \pm 1.4)$ nm agrees well with the d_{pp} for PALAS GFG soot published in the literature (7.4 nm from *Wentzel et al.* [2003] and 6.6 ± 0.9 nm from *Weingartner et al.* [1995]). Figure 3b shows the Feret diameter D_{feret} of the PCS. (D_{feret} is the diameter of the smallest possible circle circumscribed around the projection of an aggregate on the surface of the sampling support). Assuming that the aggregates on the TEM grid do not have any preferential orientation during the sampling, D_{feret} of the two-dimensional aggregate projection can be regarded, on

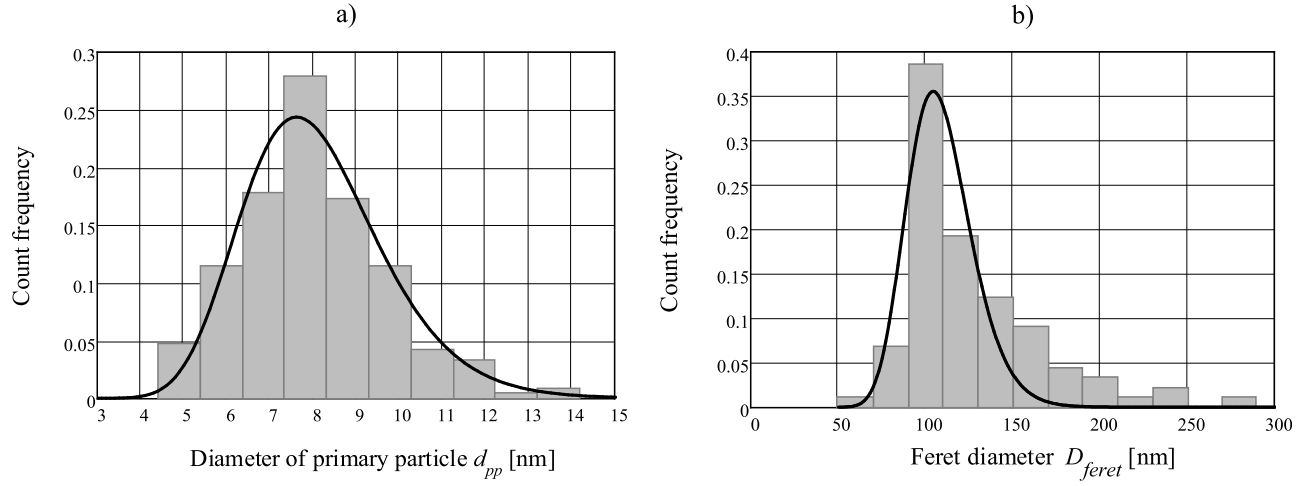

Figure 3. Frequency distributions of the morphological parameters of soot agglomerates obtained from TEM image analysis. (a) Diameter of the primary particles d_{pp} and (b) Feret diameter D_{feret} for the propanol-compacted soot. Solid lines show lognormal fit.

average, as the diameter of the smallest sphere enveloping the aggregate, D_{es}.

[15] The modal D_{feret} of the PCS particles coincides with the preselected mobility diameter of the sampled particles (100 nm). From the geometrical considerations this result is expected for ball-shaped isometric compact aggregates of spherical primary particles [*Stoeber et al.* 1970; *Kasper*, 1982]. For such agglomerates, the equality of the mobility diameter D_m and the geometrical apparent diameter, or the enveloping sphere diameter of the aggregate D_{es}, can be established [*Kasper*, 1982]. Furthermore, the apparent cluster diameter, or D_{es}, can be related to the volume equivalent diameter D_{ve} (equal to the total volume of all primary particles in the aggregate) as follows:

$$D_{es} = \left(\frac{\rho_p}{\rho_{eff}}\right)^{1/3} \cdot D_{ve}. \tag{2}$$

Here, ρ_p is the material density of the primary particles, and ρ_{eff} is the effective, or apparent density of spherical particles with diameter D_{es} having the same mass m. The compact aggregate can be now treated as a spherical particle with an apparent density defined by equation (2).

[16] To evaluate the effective density of coated particles ρ_{eff} and the mass of the coating m_{coat}, we have made an assumption that the relation (2) is also valid for the coated soot agglomerates (UCS/AHS,PCS/AHS, UCS/LG and PCS/LG) studied during LExNo. This assumption is based on the experimental finding that $D_m \approx D_{feret}$, and on the fact that the soot aggregates were compacted in all relevant cases, either with propanol prior to coating and/or with the coating due to capillary forces of the condensing substance.

3.2. Determination of Vacuum Aerodynamic Diameter D_{vae} Using LPI and AMS

[17] During LExNo, the vacuum aerodynamic equivalent diameter was determined using an LPI and two AMS instruments. The vacuum aerodynamic equivalent diameter D_{vae} was first introduced by *Jimenez et al.* [2003] as a classical aerodynamic (equivalent) diameter in the Free Molecular Regime (FMR), that is, where the characteristic size of the particle is much smaller compared to the mean free path of the surrounding gas. In FMR, a simplified expression for the Cunningham slip correction factor can be used, leading to the following simple relationship between D_{vae} and D_{ve}:

$$D_{vae} = \frac{\rho_p}{\rho_0 \cdot \chi_{FMR}} D_{ve}, \tag{3a}$$

where ρ_0 is the unit density, ρ_p is the particle density and χ_{FMR} is the dynamic shape factor of a nonspherical particle in FMR (details are given by, for example, *DeCarlo et al.* [2004], *Van Gulijk et al.* [2004], or *Schneider et al.* [2006]). Note that in (3a) the D_{ve} is defined as a volume equivalent diameter of a nonspherical particle without internal voids. For the agglomerate of spheres one has to replace the D_{ve} with D_{es} to take the empty spaces between the spheres into account. Thus, rewriting equation (3a) using D_{es} we now have

$$D_{vae} = \frac{\rho_{eff}}{\rho_0} D_{es}. \tag{3b}$$

For aggregates of small primary particles, χ_{FMR} can be expressed as a product of the envelope shape factor and the porosity [*Brockmann and Rader*, 1990; *Kelly and McMurry*, 1992]. By using D_{es} instead of D_{ve} we essentially set χ_{FMR} to 1. For moderately compact clusters as studied here the overall effect of nonsphericity is dominated by the porosity of the particles, whereas the envelope shape irregularity is responsible for the broadness of the equivalent size distributions [*Zelenyuk et al.*, 2008b]. Substituting the mobility equivalent diameter D_m for D_{es} in equation (3b), we obtain the following basic relationship for determination of the effective density of the agglomerate particles from the tandem measurements used in this study:

$$D_{vae} = \frac{\rho_{eff}}{\rho_0} D_m. \tag{3c}$$

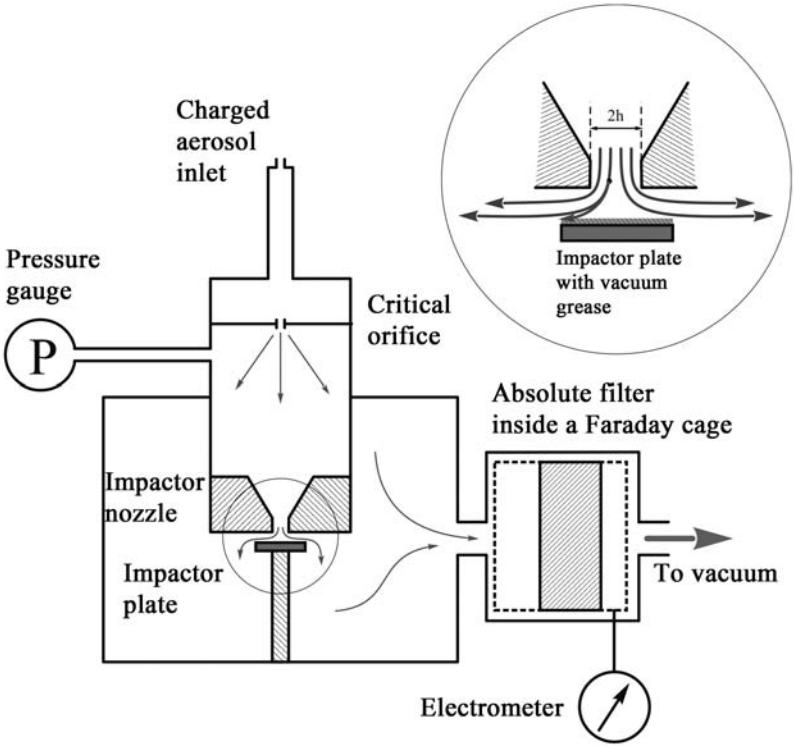

Figure 4. Schematic of LPI and the flow lines in the impactor nozzle (inset). Impaction plate was smeared with a layer of vacuum grease to avoid rebound and fragmentation of particles at high impact velocity.

Although their measurement principles differ slightly, both instruments, LPI and AMS, measure the value of D_{vae} based on the classification of particles according to their Stokes number. Whereas the AMS instruments report the D_{vae} from the measured particle velocity obtained during the acceleration in aerodynamic lenses at the entry to a high-vacuum chamber [*Allan et al.*, 2003; *Schneider et al.*, 2006], the LPI determines the critical pressure at which impaction occurs [*Fernández de la Mora et al.*, 1990; *Hering et al.*, 1978, 1979]. In practice, the LPI measures the collection efficiency of the particles as a function of pressure in the preimpaction chamber, where the pressure was gradually increased from 10 to 300 mbar. Figure 4 illustrates the operating principle of the LPI. The critical orifice between the aerosol inlet and upstream preimpactor chamber provides a constant-mass gas flow through the impactor nozzle, which directs the flow together with the unipolar charged aerosol particles onto the impaction plate. The particles that do not collide with the impaction plate transfer their charge to an absolute filter enclosed in a Faraday cage. The mirror charge induced on the Faraday cage produces an electrometer signal, which is directly proportional to the particle number concentration and number of charges on the particles. A condensation particle counter (CPC) continuously measures the particle number concentration at the inlet of the LPI. By manually varying the pressure in the chamber upstream of the impactor nozzle and recording the electrometer signal, the collection efficiency curve can be measured, and the pressure $P_{0.5}$ corresponding to the 50% collection efficiency can be determined. In the free-molecular regime (FMR, $d_p \ll \lambda$) and assuming uncompressible flow, the critical value of the Stokes number *Stk* for a particle of a given D_{vae} and unit density ρ_0 can be determined from the following relationship [*Fernández de la Mora et al.,* 1990; *Kütz*, 1994]:

$$Stk = \frac{0.178\, m\, c_0^3}{8h^3} \cdot \rho_0 D_{vae} \cdot \frac{1}{P^2} = \frac{l_{stop}}{h}, \tag{4}$$

where m is the mass flow of the gas through the nozzle, c_0 is the sonic speed, h is the impactor nozzle radius, P is the stagnation pressure in the upstream chamber of the LPI, and l_{stop} is the stopping distance. Assuming that the first term in this relation is constant for a given impactor geometry, this relation shows that the pressure in the upstream chamber of the LPI is the only parameter controlling the critical *Stk* of a particle and therefore its impaction probability [*Fernández de la Mora et al.*, 1990; *Kütz*, 1994]. Therefore, combining equations (3b) and (4) yields the following expression:

$$\rho_{eff} D_m = \rho_0 D_{vae} \sim P_{0.5}^2. \tag{5}$$

[18] According to this relation the measured value of $P_{0.5}$ can be uniquely converted into the D_{vae} of the particle, although for this conversion, the LPI must be calibrated with solid spherical particles with known density. During the LExNo experiment, the calibration of LPI was carried out using solid particles of ammonium sulfate produced by diffusion drying of sprayed droplets of $(NH_4)_2SO_4$ solution,

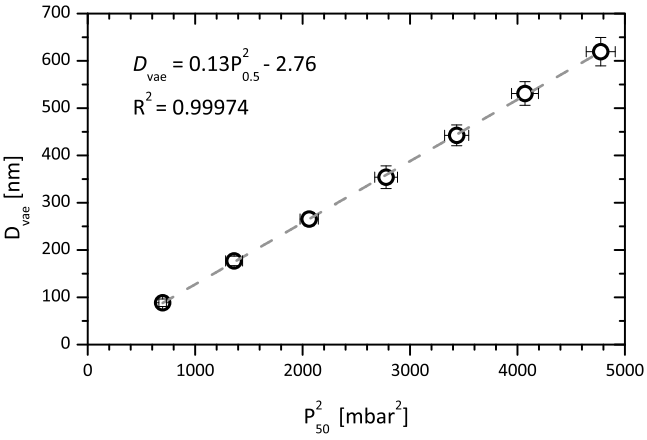

Figure 5. Calibration line of LPI obtained with solid near-spherical sulfate ammonia particles.

and then having their mobility selected using a DMA. The particles produced in this way have an almost spherical form, and thus the condition $D_m = D_{ve}$ could be used, and have a well-documented density of 1.77 g/cm^3. Figure 5 shows the calibration curve, which shows a linear fit.

[19] Figure 6 shows two examples of the collection efficiency curve, corrected for variation in the particle number concentration measured with the CPC and scaled from 0 to 1. The curves thus describe the penetration efficiency, where penetration efficiency equal to 1 is when all particles in the flow reach the filter and 0 is when all particles are collected on the impaction plate. The determination of $P_{0.5}$ and D_{vae} is straightforward if the efficiency curves look like the one in Figure 6a, namely, a simple one-step function. However, due to the presence of multiply charged particles in some cases, the efficiency curve deviates from a simple one-step function (Figure 6b). Therefore, to account for the presence of multiply charged particles, we used a 3n-parameter numerical fit algorithm in this study to estimate the value of $P_{0.5}$. This algorithm uses the fit function in the following form:

$$f(P) = \int_0^P \sum_i^n a_i e^{-\frac{1}{2}\left(\frac{t-p_i}{b_i}\right)^2} dt, \quad (6)$$

which is the sum of the n normal distributions integrated over the range of pressure values P (cumulative multimodal distribution). The number of generated normal distributions n can be varied to achieve the best fit. For sharp efficiency curves like the one in Figure 6a, a cumulative bimodal distribution was sufficient to achieve a good fit, whereas for particle systems with a high fraction of multiply charged particles, three or even four normal distributions were required to reproduce all features of the measured efficiency curve. The solid lines in Figure 6 represent the sum of the generated normal distributions calculated using the best fit values of the parameters a_i, b_i, and p_i. The value of p_1 (the modal pressure of the first normal distribution) was taken as the critical pressure $P_{0.5}$ for the singly charged particles. The fitted generated normal distributions in Figure 6 are normalized to unity.

[20] It was found that the pure solid LG particles and UCS/LG and PCS/LG particles contained a systematically larger fraction of multiply charged particles compared to the pure solid AHS particles and UCS/AHS and PCS/AHS particles. The ability of the fit algorithm to distinguish the fraction of the penetration efficiency curve responsible for the singly charged particles allowed for accurate determination of ρ_{eff} of the pure solid LG particles, which was found to be 1.58 ± 0.05, in excellent agreement with the published value of the bulk density of levoglucosan (1.6 g/cm^3). The values of ρ_{eff} obtained from the LPI and AMS size data for the other types of soot particles are discussed below.

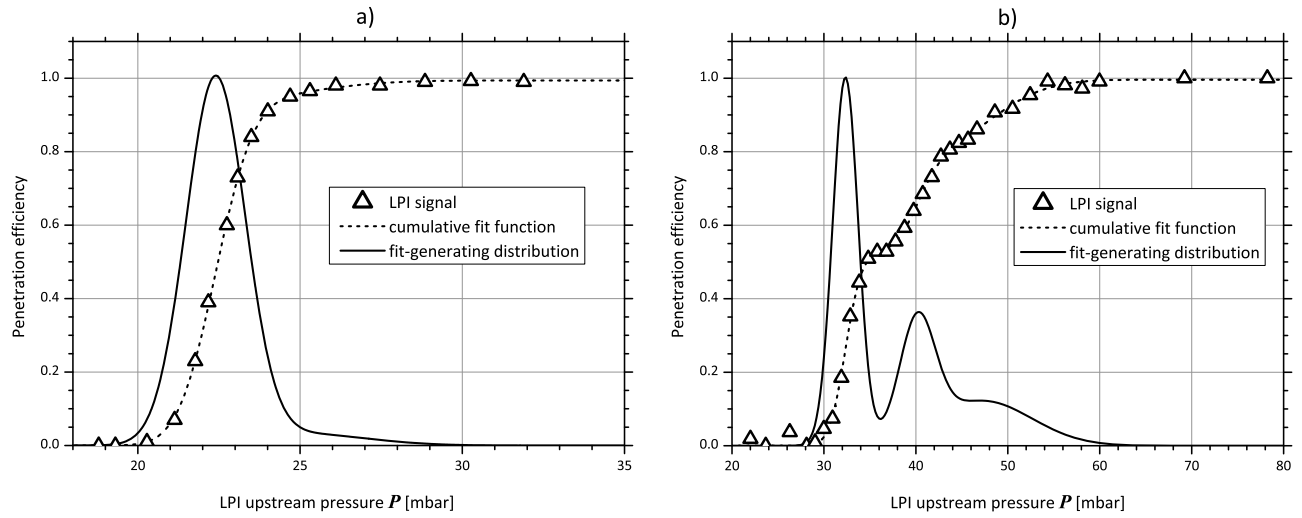

Figure 6. Two representative LPI penetration efficiency curves for (a) UCS/AHS (D_m = 100 nm, furnace temperature 140°C) and (b) pure solid levoglucosan (LG) particles with mobility diameter D_m = 90 nm. Note the significant fraction of doubly and triply charged particles leading to multiple steps in the penetration efficiency curve in Figure 6b.

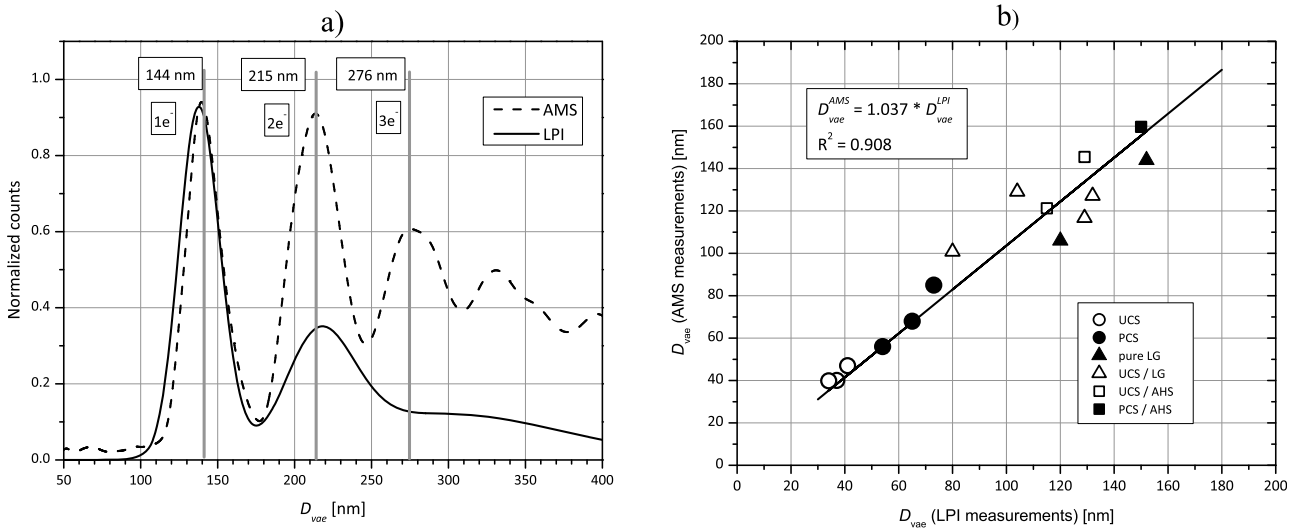

Figure 7. (a) Comparison of the vacuum aerodynamic diameter D_{vae} distribution measured with LPI and AMS for pure LG particles with the mobility diameter D_m = 90 nm (same as in Figure 6b). Bold vertical lines show D_{vae} for singly, doubly, and triply charged LG particles selected with the DMA at D_m = 90 nm. (b) Comparison of D_{vae} derived from AMS and LPI measurements for different soot types and pure substances used in the coating experiments.

3.3. Comparison of D_{vae} From the AMS Size Spectra With That From LPI Measurements

[21] The design of the AMS instruments allows for direct evaluation of the D_{vae} from the instrument signal registered in the particle time of flight (PToF) mode [*Canagaratna et al.*, 2007]. In the ideal case of solid spherical particles, the fraction of multiply charged particles with the same electrical mobility diameter is easily retrievable from the size spectra recorded with an AMS. However, the amplitude of the response signal of the AMS is proportional to the mass of the actual vaporized nonrefractory material, which, in case of particles with a complex morphology is not necessarily a function of particle size. In these cases the relative fraction of multiply charged particles cannot be readily inverted from the signal-size spectra. In contrast, the LPI response signal is proportional to the charge delivered by single particles to the electrometer and thus proportional to the number of particles multiplied by the number of charges per particle. This difference in the principle of operation of AMS and LPI means that direct comparison between D_{vae} spectra measured by these two instruments is only possible in terms of relative position of the peaks on the D_{vae} scale. Figure 7a clearly shows that both methods detected particles in the same range of D_{vae}. Moreover, the first, second and third maxima of the D_{vae} distribution coincide with the values theoretically expected for singly, doubly, and triply charged spherical particles (D_{vae} values marked with vertical lines in Figure 7a) with density equal to that of the pure bulk levoglucosan and electrical mobility diameter of 90 nm.

[22] Figure 7b summarizes the D_{vae} measurements carried out during LExNo by comparing modal D_{vae} of the singly charged particles derived from LPI and AMS measurements for different types of particles. For all particle types investigated, the aerodynamic diameters determined with the two different methods show good agreement, as indicated by a slope of 1.037 and R^2 = 0.908 for a linear fit.

3.4. Determination of Fractal Dimension D_f and Effective Density ρ_{eff}

[23] For fractal-like aggregates, the relationship between D_{vae} measured in FMR, and the D_m measured in the transition regime is as follows [*DeCarlo et al.*, 2004]:

$$D_{vae} \sim D_m^{D_f - 2}. \quad (7)$$

However, this relationship is valid only if $D_f > 2$. This limitation arises because the drag on the fractal cluster in FMR is proportional to the collision frequency between the cluster parts and the gas molecules [*Rogak*, 1991, *DeCarlo et al.*, 2004]. If the fractal dimension of the cluster is less than 2, the cluster is essentially "transparent" for the trajectories of gas molecules and therefore its aerodynamic diameter is not a function of the actual size of the agglomerate, but rather the drag depends on the size of the primary particles. In contrast, the D_m measured in the continuum regime is linearly proportional to the R_g [*Wang and Sorensen*, 1999] and therefore depends on N_{pp}. The soot particles generated in the PALAS spark discharge generator have a fractal dimension close to 2 [*Naumann*, 2003; *Wiltzius*, 1987], and therefore the evaluation of D_f from the tandem mobility and aerodynamic measurements requires measurements in the widest possible range of mobility sizes. During LExNo, the D_m of the agglomerates produced by the PALAS GFG soot generator could be varied from 50 nm to 300 nm, thus allowing determination of a relationship between D_m and D_{vae} of UCS selected by the DMA (see Figure 8). From the linear slope of the $log(D_{vae})$ plotted versus $log(D_m)$, D_f for UCS was 2.13 ± 0.05, which agrees well with the value 2.1 published in the literature [*Naumann*, 2003; *Schneider et al.*, 2006; *Weingartner et al.*, 1995; *Wiltzius*, 1987]. Uncertainty in D_f was evaluated from the uncertainty in the mean-square linear fit on a log-log scale.

[24] Similar analysis for data from the AMS size spectra reveals a slightly flatter slope of the relationship between D_{vae}

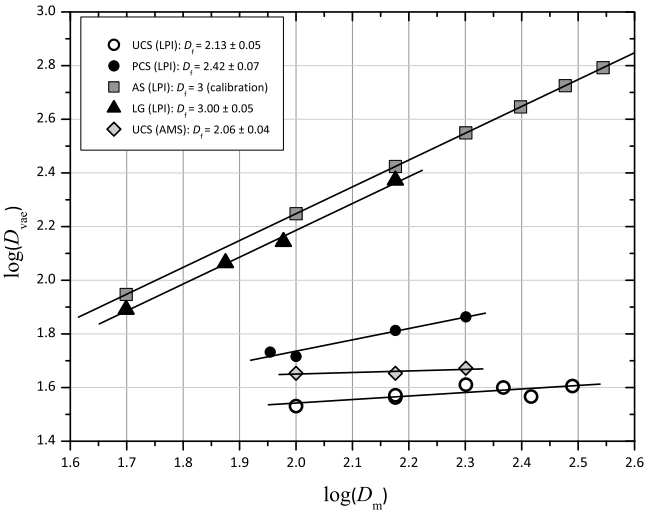

Figure 8. Determination of fractal dimension D_f of soot aggregates and solid near-spherical particles. Uncertainties were calculated from the uncertainty in the mean-square fit. Uncertainty for ammonium sulfate particles is not given because D_{vae} was calculated from preset values of D_m using equation (3b).

and D_m of the uncompacted soot agglomerates (Figure 8), but still agrees well with the LPI results. Furthermore, D_f = 2.06 ± 0.04, which again agrees well with LPI results and those in the literature, as mentioned in the preceding paragraph. Note however, that an AMS would be unable to detect UCS if it were pure graphite, therefore the measurements of UCS were possible only because volatile organic contamination from the gas phase and from the walls of the discharge chamber [*Roth et al.*, 2004] or from the tubing walls [*Schneider et al.*, 2006] was found in the soot particles. Analysis of the mass spectra identified the most abundant contaminant as dimethylsiloxane $(SiOC_2H_6)_nSiOC_2H_5^+$ (n = 0: m/z = 73), which is a constituent of silicone. A mass-to-charge ratio of 73 was therefore used as a marker for uncoated soot particles throughout the experiment.

[25] Following the same method, D_f of the PCS was measured as 2.42 ± 0.07 based on the LPI measurements of D_{vae}. To validate this method, it was additionally applied to dry aerosol particles generated by spraying aqueous solutions of the two pure coating substances (ammonium sulfate and levoglucosan) used during the LExNo experiment. Results showed that D_f for such particles was 3, according to the theory (Figure 8).

[26] Another important parameter relevant for description of soot aggregate morphology is the ρ_{eff}. The ρ_{eff} of an aggregate has a rather simple physical meaning; it is defined as the ratio of the total mass of the aggregate m_{aggr} to the volume of the envelope enclosing the aggregate. Following the argument used in the section 3.1, statistically, the envelope of the aggregate can be considered spherical, and therefore the diameter of the enveloping sphere D_{ve} can be used to express ρ_{eff} as follows:

$$\rho_{eff} = \frac{6 \cdot m_{aggr}}{\pi D_{es}^3}. \quad (8)$$

Because the mass of an aggregate is equal to the total mass of all its primary particles, ρ_{eff} can be written as

$$\rho_{eff} = \frac{N_{pp} \cdot d_{pp}^3 \cdot \rho_{bulk}}{D_{es}^3}. \quad (9)$$

For a fractal-like aggregate, N_{pp} can be calculated from equation (1) if R_g and k_f are known. According to *Sorensen and Roberts* [1997], the value of k_f can be estimated as

$$k_f = f\left[\frac{D_f}{D_f + 2}\right]^{-D_f/2}, \quad (10)$$

where f = 0.74 is the volume-filling factor accounting for the fact that even in the most closely packed agglomerate the primary particles can occupy not more than 74% of space. Based on these assumptions, k_f = 1.49 for the UCS and k_f = 1.53 for PCS.

[27] The diameter of the enveloping sphere (a three-dimensional analogue of the Feret diameter) was approximately equal to D_m of the soot aggregates (see section 3.1), and therefore, combining equations (1) and (9) yields the following relationship:

$$\rho_{eff} = k_f \cdot \left(\frac{2R_g}{d_{pp}}\right)^{D_f} \frac{d_{pp}^3 \cdot \rho_{bulk}}{D_m^3}. \quad (11)$$

[28] Finally, D_m of the fractal-like aggregates is proportional to R_g, namely, $D_m/2R_g = k_{Rg}$ [*Wang and Sorensen*, 1999], where the coefficient of proportionality k_{Rg} depends on the size distribution of the primary particles and D_f of the aggregate. Several theoretical and experimental studies give the value of k_{Rg} in the range from 0.8 to 1 [*Wang and Sorensen*, 1999]. Because this is the only structural parameter that was not directly evaluated from the experimental data, in our study it was used as an adjustment parameter to fit the theoretically calculated ρ_{eff} to the experimental data.

[29] Figure 9 shows the experimentally determined values of ρ_{eff} for UCS and PCS using the relationship $\rho_{eff} = \frac{D_m}{D_{vae}}\rho_0$, where ρ_0 is the unit density. Also plotted are the values of ρ_{eff} calculated using following the equation:

$$\rho_{eff} = \frac{k_f \cdot \rho_{bulk}}{k_{Rg}^{D_f}} \cdot \left(\frac{D_m}{d_{pp}}\right)^{D_f - 3}, \quad (12)$$

where all parameters except k_{RG} were determined either from the experimental data obtained during the LExNo campaign or calculated from this experimental data as described above.

[30] The best fit between experimental and theoretically predicted values of ρ_{eff} was achieved using k_{Rg} = 0.93 for UCS and k_{Rg} = 1.05 for PCS, both of which agree well with k_{Rg} values published by *Wang and Sorensen* [1999]. These parameters were then used to determine the mass of the coating material per particle m_{coat} as described in section 3.5.

3.5. Determination of Coating Mass per Particle m_{coat} From Effective Density ρ_{eff} Measurements

[31] The applicability of the fractal approach to the morphology analysis of the soot particles before and after compaction was clearly demonstrated in section 3.4. Based

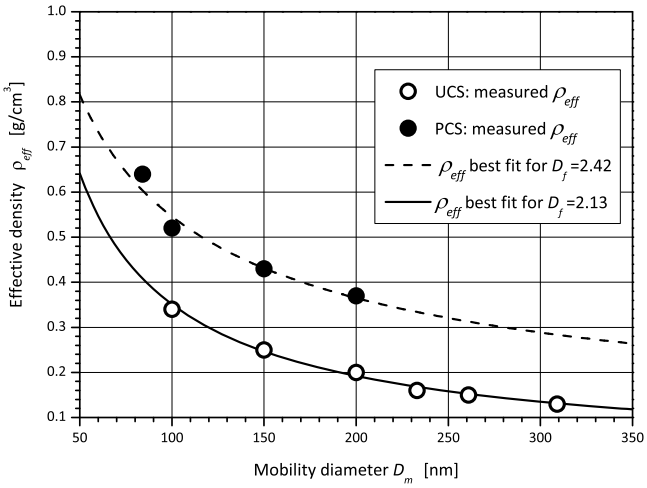

Figure 9. Effective density ρ_{eff} of uncompacted and compacted soot particles (USC and PCS, respectively) calculated from tandem measurements of mobility diameter D_m and vacuum aerodynamic diameter D_{vae}. Lines show theoretically calculated values based on the structural parameters derived from TEM measurements and fractal dimension (D_f) measurements.

on the structure parameters estimated in sections 3.3 and 3.4, m_{coat} can be determined for the different coating conditions and different states of agglomerates before the coating. The "coating" of porous soot agglomerates by condensation of a volatile substance is a combination of two processes: penetration of the condensing substance into the inner pores of the soot aggregates, and compaction of the aggregates due to surface tension forces of the condensing substance [*Mikhailov et al.*, 1999, *Ristimäki and Keskinen*, 2006]. When coating is complete, a soot particle is a relatively compact aggregate with the empty space between the primary particles fully or partially filled with the condensed coating substance, which is either AHS or LG in our case. The total mass of the coating material depends on the coating conditions (vapor pressure, exposure time and cooling temperature gradient), but there is no evidence that the coating substance forms a homogeneous layer on the surface of the compacted aggregate. This means that unless the condensing substance "overfills" the pores inside the aggregate, then the diameter of the envelope enclosing the resulting aggregate does not depend on the amount of the coating material deposited onto the agglomerate, but rather only on the restructuring leading to the formation of the compact aggregate. In our case, the enveloping sphere of a coated aggregate has the same diameter D_{es} as the enveloping sphere of an imaginary "skeleton" aggregate that has been compacted to the same extent but does not contain any coating material. Based on this assumption, m_{coat} can be estimated as the difference between the mass of two such aggregates, $m_{coat} = m_{aggr}^{coat} - m_{aggr}^{uncoat}$. Taking into account that for compact aggregates, D_{es} is, on average, approximately equal to D_m (see TEM analysis results in section 3.1), m_{coat} can be written as

$$m_{coat} = \frac{\pi}{6}\left(\rho_{aggr}^{coat} - \rho_{aggr}^{uncoat}\right) D_m^3. \tag{13}$$

As described section 3.4, the effective density of a coated aggregate ρ_{aggr}^{coat} can be evaluated from the ratio D_{vae}/D_m. The effective density of an uncoated aggregate ρ_{aggr}^{uncoat} can be calculated based on N_{pp} in the aggregate being constant and therefore the mass of the aggregate is not affected by the compaction as long as no coating is applied. Therefore,

$$\frac{\pi}{6} d_{pp}^3 \cdot N_{pp} \cdot \rho_{bulk} = \frac{\pi}{6} D_m^3 \cdot \rho_{aggr}^{uncoat} \quad \text{or} \quad \rho_{aggr}^{uncoat} = \left(\frac{d_{pp}}{D_m}\right)^3 N_{pp} \cdot \rho_{bulk}. \tag{14}$$

[32] To calculate N_{pp} we use the scaling relationship for fractal-like aggregates equation (1), where $2R_g$ has been replaced with the corrected value of D_m (see discussion in section 3.4),

$$N_{pp} = k_f \cdot \left(\frac{k_{Rg} \cdot D_m^{uncoat}}{d_{pp}}\right)^{D_f}. \tag{15}$$

In equation (14), ρ_{bulk} is the bulk density of the primary particle material, 1.85 g/cm^3 (approximate value for amorphous graphite), and D_m^{uncoat} and D_f are the D_m and D_f, respectively, of aggregates before the coating. The value of k_{Rg} was taken as 0.93 for the UCS and 1.05 for the PCS as derived from the best fit procedure described in section 3.4. Note that although D_m^{uncoat} was chosen as 100 nm for both UCS and PCS, D_f and k_f differ for these two types of particles, namely, $D_f = 2.42$ and $k_f = 1.44$ for UCS and $D_f = 2.13$ and $k_f = 1.42$ for PCS.

[33] Figure 10 shows the m_{coat} calculated using this method as a function of coating temperature in the furnace for all four main types of soot particles studied during LExNo. The instruments (LPI and AMS) used in the measurements to derive D_{vae} are indicated in the legend. The LPI measurements of UCS/LG and PCS/LG were carried

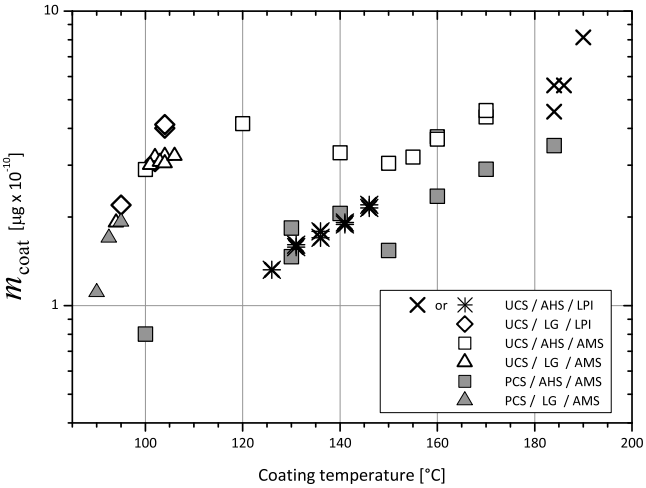

Figure 10. Coating mass m_{coat} per particle as a function of coating temperature for different types of particles (USC, PCS), coating (AHS, LG), and instruments (LPI, AMS) used for determination of vacuum aerodynamic diameter D_{vae}. Star symbols indicate UCS/AHS/LPI measurements done with a different coating furnace.

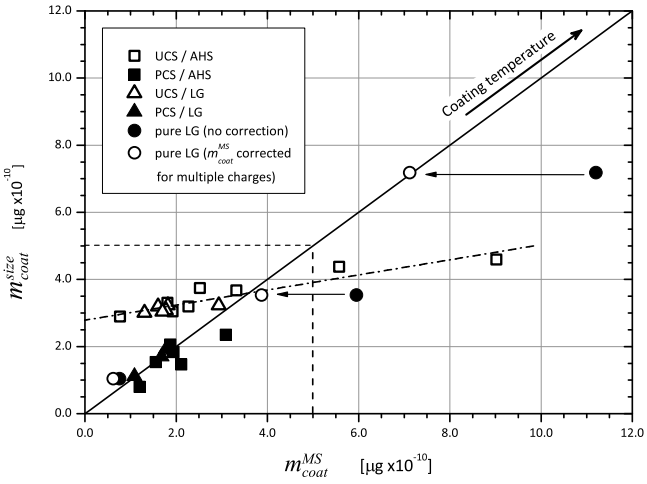

Figure 11. Comparison between m_{coat}^{size} and m_{coat}^{MS} for PCS (solid symbols) and USC (open symbols, and linear fit shown as a dash-dotted line). The "m_{coat}" of pure LG particles (values on the y axis) was calculated from the preselected mobility diameter D_m and the effective density derived from LPI measurements. Arrows point from the uncorrected to corrected values, namely, before and after "multiple charges" correction (see text). Dashed lines at $m_{coat} = 5 \times 10^{-10}\mu$g mark the upper limits of applicability of the "no-overfill" assumption. Symbols are the same as in Figure 10.

out in parallel with the AMS measurements, whereas the UCS/AHS and PCS/AHS were measured in part with the LPI (for the temperature range between 120°C and 150°C) on a different day using a slightly different coating furnace (made of glass instead of ceramic), and indicated by stars in Figure 10. Otherwise the particle generation and coating conditions were identical.

[34] Several features of the coating behavior can be recognized in Figure 10. First, m_{coat} clearly increases with the coating temperature, for both the AHS and LG coatings. Second, m_{coat} is approximately the same for both the AHS and LG coatings. Third, m_{coat} for AHS derived from the D_{vae} from AMS size spectra (open and closed squares in Figure 10) is relatively scattered, indicating a larger day-to-day variability than the values calculated from the D_{vae} measurements made with LPI (crosses and stars). Fourth, m_{coat} for AHS is higher for USC (open symbols) compared to PCS (closed symbols). This fourth feature is expected considering that the PCS have almost double the number of primary particles for the same mobility size and thus have a smaller amount of empty space between the primary particles to accumulate the coating substance. However, this effect of the compaction of soot is more distinct for LPI-obtained m_{coat} values compared to values obtained from the AMS mass spectra data as shown in Figure 1 of the companion paper by *Henning et al.* [2010] (see also quantitative analysis in section 3.6). In the case of LG coating the difference between uncompacted and compacted soot is not as distinctive due to the lack of experimental data for the same coating regimes.

[35] The uncertainties in D_f, k_f, and k_{Rg} can be directly related to uncertainty in the mass of the "skeleton" soot aggregate m_{aggr}^{uncoat}. Therefore the relative contribution of these uncertainties to the uncertainty in m_{coat} depends on the amount of coating applied to the aggregate and on the state of the aggregate (compacted or uncompacted) before the coating was applied. In UCS/AHS and UCS/LG, m_{coat} is relatively insensitive to the slight variations in morphological parameters: variation in D_f and $k_f = f(D_f)$ according to (10) within the experimental uncertainties of D_f translates into 3 to 10% variation in m_{coat}, which for PCS/AHS and PCS/LG translates into a variation in m_{coat} of up to 30%. Variation in k_{Rg} within 10% of its magnitude translates into 3% to 7% variation in m_{coat} for UCS/AHS and UCS/LG, and into 13% to 50% variation if the coating was for PCS/AHS and PCS/LG.

3.6. Comparison of m_{coat} Obtained Using Two Different Methods From AMS Measurements

[36] Utilization of nonrefractory soot particles as a carrier for volatile coating material provides a unique opportunity to compare m_{coat} evaluated using two different methods from measurements made with the same AMS instrument. The first method is to derive m_{coat} from the vacuum aerodynamic equivalent diameter measurements as described in section 3.5, and the second is to derive it by dividing the mass concentration of the nonrefractory compounds inferred from the recorded mass spectra by the particle concentration measured with a CPC. Hereafter we refer to the first method as a "size-based method," and to the second method as a "mass-spectra-based method." To differentiate between the coating mass per particle obtained with these two methods we use different notations, m_{coat}^{size} and m_{coat}^{MS}, respectively. Figure 11 compares the results from these two methods.

[37] The overall agreement between m_{coat}^{size} and m_{coat}^{MS} is amazingly good considering the principal difference between the methods, the irregularity of soot particle morphology, and the broadness of the size distribution. However, the different behavior for compacted and uncompacted particles is even more pronounced in Figure 11 compared with data of Figure 10. Whereas the values for m_{coat}^{size} and m_{coat}^{MS} agree well for uncoated PCS (solid symbols in Figure 11), the values of m_{coat}^{size} for UCS are higher than m_{coat}^{MS} for UCS.

[38] The nature of this discrepancy is not definitively clear. It cannot be explained by the presence of doubly charged particles because such particles would produce a reverse effect, namely, the values of m_{coat}^{MS} would have been higher than m_{coat}^{size} and thus would have appeared below the 1:1 line. Note here that the AMS data were processed using a collection efficiency (fraction of particles that are flash-evaporated on the vaporizer compared to the total number of particles striking the vaporizer) of unity. A possible reason for systematic disagreement might be that the porous structure of the soot agglomerates prevents evaporation of the entire mass of the coating material during the thermal vaporization of the particles in the AMS, thus making the collection efficiency less than unity, and, furthermore, structure-dependent. This effect would lead to underestimation of the m_{coat}^{MS} values. On the other hand, this effect would explain why the agreement between m_{coat}^{size} and m_{coat}^{MS} is better for the PCS; the agglomerates that have been compacted prior to coating have their inner space unavailable for condensation of the coating substance, thus the coating is

concentrated near the surface of the agglomerate. This makes the coating material more readily available for vaporization, whereas the coating substance inside the originally loose agglomerates is "protected" from the high-temperature environment during the evaporation stage in the AMS. This effect would seem to be independent from the type of coating substance (no systematic difference between the LG and AHS coated soot is evident in Figure 11).

[39] However, two measurement points for the UCS/AHS (open squares above 5×10^{-10} μg in Figure 11) do not conform with this hypothesis. For these two measurements the values of m_{coat}^{MS} are significantly higher than values of m_{coat}^{size}. This deviation from the otherwise consistent behavior might be understood as a violation of the underlying assumption used in the evaluation of the m_{coat}, stating that the condensing material does not "overfill" the aggregate (see section 3.5). The "critical" mass m_{crit} of the condensed material that can fill the spaces between the monomers without projecting from the envelope of a coated aggregate with diameter D_m^{coat} is given by the simple relationship

$$m_{crit} = \frac{\pi}{6} \cdot \left[\left(D_m^{coat} \right)^3 - N_{pp} \cdot d_p^3 \right] \cdot \rho_{AHS} \qquad (16)$$

and can be evaluated using equation (15), which relates the N_{pp} of the uncoated soot aggregate to its mobility size D_m^{uncoat}. Assuming D_m^{uncoat} = 100 nm and using D_f = 2.13, k_{Rg} = 0.93, and k_f = 1.42 as calculated in section 3.4, and also assuming ρ_{AHS} = 1.77 g/cm^3, we obtain m_{crit} on the order of 5×10^{-10} μg. This clearly shows that these two measurement data points lie outside the range of validity for the "no-overfill" assumption used in the discussion in section 3.5 and marked by the dashed lines in the Figure 11. Therefore, the size-based method significantly underestimates m_{coat}^{size} compared to the m_{coat}^{size} determined using the direct measurements of vaporized material with the AMS.

[40] Figure 11 also reveals that if no correction is made for the presence of multiply charged particles, the m_{coat}^{MS} for pure LG particles derived from the AMS mass spectra would be almost a factor of 2 higher than that predicted using equation (3b) for a given mobility size D_m of dry LG particles and a bulk density of 1.6 g/cm^3 (solid circles in Figure 11). This disagreement is a consequence of the calculation procedure used to evaluate m_{coat}^{MS}, in which the mass concentration of the evaporated compound (which is the total mass of all LG particles in a unit volume in this case) is divided by the particle number concentration. Because the population of LG particles contained a considerable fraction of multiply charged particles (see Figure 6b and section 3.3) such a procedure produces a significant deviation in m_{coat}^{MS} from the value expected for a given D_m and particle density ρ_{eff}. However, evaluating the fraction of the total mass delivered by singly charged particles from the AMS size spectra and, evaluating their number concentration independently from the LPI data m_{coat} of a singly charged pure solid LG particle can be determined. After this correction, the average mass of the LG particles (open circles in Figure 11) was similar to the expected mass of the spherical particles having a preset mobility size D_m and ρ_{eff} equal to the density of the pure solid LG (arrows point from the uncorrected to corrected values, namely, before and after this "multiple charges" correction).

4. Summary and Conclusions

[41] Tandem mobility-aerodynamic measurements were used to provide information on particle morphology during the LExNo experiment on the hygroscopic growth and activation of model soot aerosol. These measurements were supported with data obtained by transmission electron microscopy (TEM). The soot particles studied in this work were produced in a spark discharge generator and were coated with ammonium hydrogen sulfate (AHS) or levoglucosan (LG) to increase the hygroscopic activity of originally nonhygroscopic mostly graphite aggregates. Using a custom-made, single-stage low-pressure impactor (LPI) and two time-of-flight mass spectrometers (AMS) operating in the free molecular regime, the vacuum aerodynamic diameter D_{vae} of the mobility-selected soot particles was measured for uncompacted soot (UCS), for soot compacted with propanol (PCS) and for UCS and PCS coated with one of the two coating substances (AHS or LG). From these measurements, the fractal dimension D_f, the effective density ρ_{eff} and the average mass of the coating material per particle m_{coat} were derived. The m_{coat} was also compared to that obtained from the AMS mass spectra, m_{coat}^{MS}.

[42] The manual mode of the LPI operation and stability of the particle generation equipment allowed for careful determination of the vacuum aerodynamic equivalent diameter D_{vae} of the soot agglomerates with different morphology. Due to the time-consuming nature of the LPI measurements in the manual mode the LPI measurements could not be conducted on a regular basis and were only made when sufficient particle number concentration was available. Nevertheless, the simultaneous measurements of D_{vae} with LPI and AMS instruments, where available, showed good agreement.

[43] Results demonstrated that the suggested multiparameter fit procedure of the penetration efficiency curves allows for accurate determination of the critical pressure corresponding to the cutoff aerodynamic diameter of the LPI, even when a significant fraction of multiply charged particles is present. This provides high sensitivity to a method to determine the mass of the particle and, when combined with the measurement of its mobility size D_m, its ρ_{eff}, as shown in the case of pure LG particles.

[44] The fractal analysis applied to data obtained from the tandem mobility/aerodynamic measurements revealed structure parameter values that are characteristic for soot agglomerates from a PALAS GFG-1000 spark discharge generator. Despite the relatively narrow size range analyzed, D_f for the uncompacted GFG soot (UCS) was 2.13, which agrees well with values reported in the literature. The D_f value of 2.42 for PCS indicates that soot aggregates do not undergo a complete collapse of the inner structure, which would result in a D_f value close to 3. The compaction of soot agglomerates was confirmed by TEM images of individual agglomerates sampled during the LExNo experiment. These images were used to determine the size distribution of primary particles comprising the agglomerates. This size

distribution, together with knowledge of the modal D_m, allowed for evaluation of the average number of primary particles N_{pp} per aggregate and the fractal prefactor k_f. Both quantities determined here are consistent with those obtained from the literature.

[45] By using these morphological parameters, further analysis revealed that the relationship between ρ_{eff} and D_f of uncompacted and compacted soot agglomerates has a simple exponential form as predicted by theory for fractal-like agglomerates of small particles. So that shape-relevant information could be excluded, an effective density was introduced as the mass of the aggregate divided by the volume of a sphere that envelopes the aggregate. This allowed for determination of ρ_{eff} from the ratio of D_{vae} to D_m, despite both quantities being experimentally measured in different pressure regimes (transition regime in the DMA and free molecular regime in the LPI and AMS instruments).

[46] Within this tandem measurement approach, m_{coat} was evaluated for the two coating substances and for several temperature regimes of coating. Results demonstrated that the tandem mobility-aerodynamic measurements with LPI or AMS instruments are sufficiently sensitive to detect coating-induced changes in the particle effective density and morphology. The m_{coat} values exhibit physically self-consistent behavior, that is (1) gradual increase in m_{coat} with increasing coating temperature in the furnace and (2) clearly higher m_{coat} deposited onto UCS compared to PCS before coating. The m_{coat} values calculated from the LPI measurement data showed overall less scattering, so that the statistically significant increase in m_{coat} is clearly evident even in the furnace temperature interval of several degrees Celsius.

[47] The m_{coat}^{size} values calculated from D_{vae} data of the AMS were compared to the mass of the nonrefractory material (m_{coat}^{MS}) derived from the AMS mass spectra. The size-based and mass spectra–based methods showed good agreement, considering the principal difference in the two techniques and the complex morphology of the soot agglomerates. However, m_{coat}^{MS} values do not exhibit significant differences between PCS and UCS, whereas m_{coat}^{size} values are clearly higher for the UCS compared with PCS. One possible explanation is that the precompacted agglomerates have a smaller volume of voids that could be filled with the coating substance. Therefore, underestimation of m_{coat} derived from the mass spectra could be a feature inherent to the thermal vaporization technique utilized in the AMS instruments when applied to highly porous agglomerates of mostly nonrefractory particles (carbon) with the refractory mass concealed in the inner voids. The inconsistency in two measurement points with this explanation was interpreted as a violation of the underlying assumption used in the method to calculate m_{coat}, namely, that the condensing material does not overfill the pores inside the aggregate and therefore does not change the envelope size of the aggregate.

References

Allan, J. D., J. L. Jimenez, P. I. Williams, M. R. Alfarra, K. N. Bower, J. T. Jayne, H. Coe, and D. R. Worsnop (2003), Quantitative sampling using an Aerodyne aerosol mass spectrometer: 1. Techniques of data interpretation and error analysis, *J. Geophys. Res.*, *108*(D3), 4090, doi:10.1029/2002JD002358.

Brockmann, J. E., and D. J. Rader (1990), APS response to nonspherical particles and experimental-determination of dynamic shape factor, *Aerosol Sci. Technol.*, *13*, 162–172, doi:10.1080/02786829008959434.

Canagaratna, M. R., et al. (2007), Chemical and microphysical characterization of ambient aerosols with the aerodyne aerosol mass spectrometer, *Mass Spectrom. Rev.*, *26*, 185–222, doi:10.1002/mas.20115.

DeCarlo, P. F., et al. (2004), Particle morphology and density characterization by combined mobility and aerodynamic diameter measurements. Part 1: Theory, *Aerosol Sci. Technol.*, *38*, 1185–1205. (Erratum, *Aerosol Sci. Technol.*, *39*, 184–184, 2005).

Fernández de la Mora, J. F., et al. (1990), Inertial impaction of fine particles at moderate Reynolds numbers and in the transonic regime with a thin-plate orifice nozzle, *J. Aerosol Sci.*, *21*, 889–909, doi:10.1016/0021-8502(90)90160-Y.

Geller, M., et al. (2006), Determination of particle effective density in urban environments with a differential mobility analyzer and aerosol particle mass analyzer, *Aerosol Sci. Technol.*, *40*, 709–723, doi:10.1080/02786820600803925.

Helsper, C., et al. (1993), Investigations of a new aerosol generator for the production of carbon aggregate particles, *Atmos. Environ., Part A*, *27*, 1271–1275.

Henning, S., et al. (2010), Soluble, mass, hygroscopic growth, and droplet activation of coated soot particles during LACIS Experiment in November (LExNo), *J. Geophys. Res.*, *115*, D11206, doi:10.1029/2009JD012626.

Hering, S. V., et al. (1978), Design and evaluation of new low-pressure impactor. 1, *Environ. Sci. Technol.*, *12*, 667–673, doi:10.1021/es60142a004.

Hering, S. V., et al. (1979), Design and evaluation of a new low-pressure impactor. 2, *Environ. Sci. Technol.*, *13*, 184–188, doi:10.1021/es60150a009.

Jimenez, J. L., R. Bahreini, D. R. Cocker III, H. Zhuang, V. Varutbangkul, R. C. Flagan, J. H. Seinfeld, C. D. O'Dowd, and T. Hoffmann (2003), New particle formation from photooxidation of diiodomethane (CH_2I_2), *J. Geophys. Res.*, *108*(D10), 4318, doi:10.1029/2002JD002452.

Kasper, G. (1982), Dynamics and measurement of smokes. 1. Size characterization of non-spherical particles, *Aerosol Sci. Technol.*, *1*, 187–199, doi:10.1080/02786828208958587.

Kelly, W. P., and P. H. McMurry (1992), Measurement of particle density by inertial classification of differential mobility analyzer generated monodisperse aerosols, *Aerosol Sci. Technol.*, *17*, 199–212, doi:10.1080/02786829208959571.

Kütz, S. (1994), In-situ Methoden zur Bestimmung von Struktureigenschaften gasgetragener Agglomerate, Ph.D. thesis, Univ. of Duisburg-Essen, Duisburg, Germany.

Kütz, S., and A. Schmidt-Ott (1990), Use of a low-pressure impactor for fractal analysis of submicron particles, *J. Aerosol Sci.*, *21*, Suppl. 1, S47–S50, doi:10.1016/0021-8502(90)90186-2.

McMurry, P. H., et al. (2002), The relationship between mass and mobility for atmospheric particles: A new technique for measuring particle density, *Aerosol Sci. Technol.*, *36*, 227–238, doi:10.1080/027868202753504083.

Messerer, A., et al. (2003), Thermophoretic deposition of soot aerosol particles under experimental conditions relevant for modem diesel engine exhaust gas systems, *J. Aerosol Sci.*, *34*, 1009–1021, doi:10.1016/S0021-8502(03)00081-8.

Mikhailov, E. F., et al. (1999), Soot particle restructuring due to interaction with water droplets, *J. Aerosol Sci.*, *30*, S443–S444, doi:10.1016/S0021-8502(99)80233-X.

Mikhailov, E. F., et al. (2001), Interaction of soot aerosol particles with water droplets: influence of surface hydrophilicity, *J. Aerosol Sci.*, *32*, 697–711, doi:10.1016/S0021-8502(00)00101-4.

Naumann, K. H. (2003), COSIMA—A computer program simulating the dynamics of fractal aerosols, *J. Aerosol Sci.*, *34*, 1371–1397, doi:10.1016/S0021-8502(03)00367-7.

Park, K., et al. (2003a), Relationship between particle mass and mobility for diesel exhaust particles, *Environ. Sci. Technol.*, *37*, 577–583, doi:10.1021/es025960v.

Park, K., et al. (2003b), A closure study of aerosol mass concentration measurements: comparison of values obtained with filters and by direct measurements of mass distributions, *Atmos. Environ.*, *37*, 1223–1230, doi:10.1016/S1352-2310(02)01016-6.

Park, K., et al. (2008), Tandem measurements of aerosol properties—A review of mobility techniques with extensions, *Aerosol Sci. Technol.*, *42*, 801–816, doi:10.1080/02786820802339561.

Ristimäki, J., and J. Keskinen (2006), Mass measurement of non-spherical particles: TDMA-ELPI setup and performance tests, *Aerosol Sci. Technol.*, *40*, 997–1001, doi:10.1080/02786820600910779.

Ristimäki, J., et al. (2002), On-line measurement of size distribution and effective density of submicron aerosol particles, *J. Aerosol Sci.*, *33*, 1541–1557, doi:10.1016/S0021-8502(02)00106-4.

Rogak, S. N. (1991), Aerosol dynamics of agglomerates, Ph.D. thesis, Calif. Inst. of Technol., Pasadena.

Roth, C., et al. (2004), Generation of ultrafine particles by spark discharging, *Aerosol Sci. Technol.*, *38*, 228–235, doi:10.1080/02786820490247632.

Schmid, O., et al. (2007), On the effective density of non-spherical particles as derived from combined measurements of aerodynamic and mobility equivalent size, *J. Aerosol Sci.*, *38*, 431–443, doi:10.1016/j.jaerosci.2007.01.002.

Schmidt-Ott, A. (1988a), In situ measurement of the fractal dimensionality of ultrafine aerosol particles, *Appl. Phys. Lett.*, *52*, 954–956, doi:10.1063/1.99239.

Schmidt-Ott, A. (1988b), New approaches to in situ characterization of ultrafine agglomerates, *J. Aerosol Sci.*, *19*, 553–563, doi:10.1016/0021-8502(88)90207-8.

Schneider, J., et al. (2006), Mass spectrometric analysis and aerodynamic properties of various types of combustion-related aerosol particles, *Int. J. Mass Spectrom.*, *258*, 37–49, doi:10.1016/j.ijms.2006.07.008.

Slowik, J. G., et al. (2004), Particle morphology and density characterization by combined mobility and aerodynamic diameter measurements. Part 2: Application to combustion-generated soot aerosols as a function of fuel equivalence ratio, *Aerosol Sci. Technol.*, *38*, 1206–1222, doi:10.1080/027868290903916.

Snider, J. R., et al. (2010), Intercomparison of cloud condensation nuclei and hygroscopic fraction measurements: Coated soot particles investigated during the LACIS Experiment in November (LExNo), *J. Geophys. Res.*, *115*, D11205, doi:10.1029/2009JD012618.

Sorensen, C. M., and G. C. Roberts (1997), The prefactor of fractal aggregates, *J. Colloid Interface Sci.*, *186*, 447–452, doi:10.1006/jcis.1996.4664.

Stoeber, W., et al. (1970), Der aerodynamische Durchmesser von Latexaggregaten und Asbestfasern, *Staub Reinhalt. Luft*, *30*(7), 277–316.

Stratmann, F., et al. (2004), Laboratory studies and numerical simulations of cloud droplet formation under realistic supersaturation conditions, *J. Atmos. Oceanic Technol.*, *21*, 876–887, doi:10.1175/1520-0426(2004)021<0876:LSANSO>2.0.CO;2.

Stratmann, F., et al. (2010), Examination of laboratory-generated coated soot particles: An overview of the LACIS Experiment in November (LExNo) campaign, *J. Geophys. Res.*, *115*, D11203, doi:10.1029/2009JD012628.

Van Gulijk, C., et al. (2004), Measuring diesel soot with a scanning mobility particle sizer and an electrical low-pressure impactor: Performance assessment with a model for fractal-like agglomerates, *J. Aerosol Sci.*, *35*, 633–655, doi:10.1016/j.jaerosci.2003.11.004.

Wang, G. M., and C. M. Sorensen (1999), Diffusive mobility of fractal aggregates over the entire Knudsen number range, *Phys. Rev. E*, *60*, 3036–3044, doi:10.1103/PhysRevE.60.3036.

Weingartner, E., et al. (1995), Growth and structural-change of combustion aerosols at high relative-humidity, *Environ. Sci. Technol.*, *29*, 2982–2986, doi:10.1021/es00012a014.

Wentzel, M., et al. (2003), Transmission electron microscopical and aerosol dynamical characterization of soot aerosols, *J. Aerosol Sci.*, *34*, 1347–1370, doi:10.1016/S0021-8502(03)00360-4.

Wiltzius, P. (1987), Hydrodynamic behavior of fractal aggregates, *Phys. Rev. Lett.*, *58*, 710–713, doi:10.1103/PhysRevLett.58.710.

Zelenyuk, A., et al. (2006), From agglomerates of spheres to irregularly shaped particles: Determination of dynamic shape factors from measurements of mobility and vacuum aerodynamic diameters, *Aerosol Sci. Technol.*, *40*, 197–217, doi:10.1080/02786820500529406.

Zelenyuk, A., et al. (2008a), Simultaneous measurements of individual ambient particle size, composition, effective density, and hygroscopicity, *Anal. Chem.*, *80*, 1401–1407, doi:10.1021/ac701723v.

Zelenyuk, A., et al. (2008b), A new real-time method for determining particles' sphericity and density: application to secondary organic aerosol formed by ozonolysis of alpha-pinene, *Environ. Sci. Technol.*, *42*, 8033–8038, doi:10.1021/es8013562.

S. Henning, A. Kiselev, F. Stratmann, C. Wennrich, and H. Wex, Institute for Tropospheric Research, Department of Physics, Permoser Str. 15, D-04318, Leipzig, Germany.

A. Kiendler-Scharr and T. F. Mentel, ICG-II: Troposphere, Research Centre Juelich, D-52425 Juelich, Germany.

I. Lieberwirth, Max Planck Institute for Polymer Research, D-55128 Mainz, Germany.

J. Schneider and S. Walter, Particle Chemistry Department, Max Planck Institute for Chemistry, Joh.-Joachim-Becher Weg 27, D-55128 Mainz, Germany.